J Neurophysiol 121: 1938–1952, 2019.
First published March 27, 2019; doi:10.1152/jn.00113.2019.

RESEARCH ARTICLE | *Sensory Processing*

V1 microcircuit dynamics: altered signal propagation suggests intracortical origins for adaptation in response to visual repetition

Jacob A. Westerberg, Michele A. Cox, Kacie Dougherty, and Alexander Maier
Department of Psychology, Center for Integrative and Cognitive Neuroscience, and Vanderbilt Vision Research Center, Vanderbilt University, Nashville, Tennessee

Submitted 19 February 2019; accepted in final form 25 March 2019

Westerberg JA, Cox MA, Dougherty K, Maier A. V1 microcircuit dynamics: altered signal propagation suggests intracortical origins for adaptation in response to visual repetition. *J Neurophysiol* 121: 1938–1952, 2019. First published March 27, 2019; doi:10.1152/jn.00113.2019.—Repetitive visual stimulation profoundly changes sensory processing in the primary visual cortex (V1). We show how the associated adaptive changes are linked to an altered flow of synaptic activation across the V1 laminar microcircuit. Using repeated visual stimulation, we recorded layer-specific responses in V1 of two fixating monkeys. We found that repetition-related spiking suppression was most pronounced outside granular V1 layers that receive the main retinogeniculate input. This repetition-related response suppression was robust to alternating stimuli between the eyes, in line with the notion that repetition-related adaptation is predominantly of cortical origin. Most importantly, current source density (CSD) analysis, which provides an estimate of local net depolarization, revealed that synaptic processing during repeated stimulation was most profoundly affected within supragranular layers, which harbor the bulk of corticocortical connections. Direct comparison of the temporal evolution of laminar CSD and spiking activity showed that stimulus repetition first affected supragranular synaptic currents, which translated into a reduction of stimulus-evoked spiking across layers. Together, these results suggest that repetition induces an altered state of intracortical processing that underpins visual adaptation.

NEW & NOTEWORTHY Our survival depends on our brains rapidly adapting to ever changing environments. A well-studied form of adaptation occurs whenever we encounter the same or similar stimuli repeatedly. We show that this repetition-related adaptation is supported by systematic changes in the flow of sensory activation across the laminar cortical microcircuitry of primary visual cortex. These results demonstrate how adaptation impacts neuronal interactions across cortical circuits.

cortical lamination; macaque; repetition suppression; visual cortex

INTRODUCTION

Our visual system relies on prior experiences to derive behaviorally relevant interpretations from sensory information (Helmholtz 1867). One well-studied, experience-related brain process is the reduction of neuronal responses during repetitions of the same or similar stimuli (see Barron et al. 2016 for review). On the level of cortical neurons, this aspect of visual adaptation is commonly referred to as repetition suppression and is observed across many visual areas (Baylis and Rolls 1987; Kaliukhovich and Vogels 2014; Kobatake and Tanaka 1994; Li et al. 1993; Liu et al. 2009; McMahon and Olson 2007; Miller et al. 1991, 1993; Miller and Desimone 1994; Riches et al. 1991; Sawamura et al. 2006; Sobotka and Ringo 1994, 1996). Repetition suppression occurs even if the repeating stimuli are not identical (Liu et al. 2009), although the magnitude of suppression gradually falls off with decreasing stimulus similarity (Sobotka and Ringo 1994). Thus repetition suppression consists of both a stimulus-specific as well as a generalized adaptive component (Kohn 2007) that occurs under a wide variety of circumstances (Riches et al. 1991). This generalized component is of particular interest because it broadly affects cortical areas regardless of their respective response preferences (Sawamura et al. 2006).

The neuronal origins of visual adaptation are thought to originate in the primary visual cortex, or V1 (Kohn 2007), from which it spreads to other areas (King et al. 2016). However, V1 neurons do not form a homogenous entity. Instead, V1 harbors an intricate neural circuit that spatially separates the bulk of sensory inputs from the bulk of intracortical processing into different laminae (Anderson and Martin 2009; Felleman and Van Essen 1991; Garey and Powell 1971; Glickstein et al. 1967; Markov et al. 2014; Mignard and Malpeli 1991; Rockland and Pandya 1979; Rockland and Virga 1989). How repetition suppression arises within this laminar circuit is largely unknown. Specifically, although it is clear that stimulus repetition differentially affects both spiking activity and neuronal synchrony across V1 layers (Hansen and Dragoi 2011), in which layers these adaptive processes originate remains an open question.

In this study, we directly compared adaptive changes between synaptic inputs and spiking outputs to trace the primary site of adaptive modulation within V1's laminar microcircuit. As expected, we found that stimulus repetitions yielded reduced firing rates across all V1 layers. This repetition suppression was largest in supragranular layers (layers 2/3). Current source density (CSD) analysis, which provides an estimate of local net depolarization, revealed that the largest decrease in synaptic activity following stimulus repetition was located in the supragranular layers as well. Direct comparison between the temporal evolution of CSD and single-unit spiking showed that significant repetition-induced activity changes first emer-

Address for reprint requests and other correspondence: A. Maier, 111 21st Ave. South, Wilson Hall 301, Nashville, TN 37240 (e-mail: alex.maier@vanderbilt.edu).

ged in supragranular CSD. This adaptation of CSD preceded any significant reductions in spiking. Stimulating one eye and testing for repetition in the other yielded a similar adaptive response, despite the fact that different populations of upstream neurons were activated by the stimuli. These results suggest that the primary origin of repetition-related response adaptation in V1 is linked to intracortical processing within its supragranular layers.

MATERIALS AND METHODS

Animal care and surgical procedures. Two adult monkeys (*Macaca radiata*), one female (*monkey I34*) and one male (*monkey E48*) were used in this study. All procedures were in compliance with regulations set by the Association for the Assessment and Accreditation of Laboratory Animal Care, approved by Vanderbilt University's Institutional Animal Care and Use Committee, and followed National Institutes of Health guidelines. In a series of surgeries, each monkey was implanted with a custom-designed MRI-compatible head post and a plastic recording chamber (Crist Instrument) situated over dorsal striate cortex, posterior to the lunate sulcus (V1). All surgeries were performed under sterile surgical conditions using isoflurane anesthesia (1.5–2.0%), following induction with an intramuscular injection of ketamine hydrochloride (10 mg/kg). Vital signs, including blood pressure, heart rate, pulse O_2 saturation, CO_2, respiratory rate, and body temperature, were monitored continuously. During surgery, the head post and recording chamber were attached to the skull using transcranial ceramic screws (Thomas Recording) and self-curing denture acrylic (Lang Dental). Furthermore, a craniotomy was performed over the perifoveal visual field representation of V1, concurrent with the position of the recording chamber. Each monkey was given analgesics and antibiotics for postsurgical care.

Behavioral task and visual stimulation. Monkeys passively fixated within a 1° radius around a central fixation dot. All stimuli were presented with a 20-in. cathode ray tube monitor (Diamond Plus 2020u; Mitsubishi Electric) operating at 60 or 85 Hz. We used a custom mirror stereoscope so that stimuli could be presented to either eye using either the left or the ride side of the monitor (Fig. 1*A*). Stimuli were generated using MonkeyLogic (Asaad and Eskandar 2008) for MATLAB (versions R2012, R2014a; The MathWorks). After a 300-ms fixation period, a sequence of five static, sinusoidal stimuli of equivalent size, spatial frequency, and phase with variable orientation (randomly chosen, 0–175° offset from vertical) were presented while the monkey maintained fixation (Fig. 1, *B*–*C*). Although identical stimuli sometimes repeated due to the randomness of the stimulus selection, we restrict the focus of this study to the adaptive effects of stimulus repetition that occur regardless of specific stimulus orientation. Aside from orientation, we selected stimulus parameters that evoked the largest overall response, although none of these parameters were optimized for individual neurons. Selection of exact values for the stimulus parameters as well as spatial location of the stimuli (Fig. 1*D*) was evaluated by listening to the auditory multiunit activity (MUA) to a wider variety of stimuli across several randomly chosen electrode contacts (0.5–3 cycles/deg at 2–7 degrees of visual angle eccentricity). In the "short" stimulation duration condition, each stimulus in the sequence was presented for 200 ms. In the "long" stimulation duration condition, each stimulus was presented for 500 ms. Both conditions featured a 200-ms interstimulus interval (ISI) between each stimulus. Following 200 ms after the last stimulus of each sequence, the monkey was relieved from the constraint of fixation and received a juice reward. If at any point during the trial (i.e., stimulus sequence) the monkey broke fixation or blinked, the trial was aborted and the monkey experienced a short (1–5 s) timeout before starting the next trial.

Neurophysiological procedure. Broadband (0.5 Hz to 12.207 kHz) intracranial voltage fluctuations were recorded across 61 experimental sessions inside an electromagnetic radiofrequency-shielded booth with an acute laminar multielectrode array. Voltages were amplified, filtered, and digitized using the 128-channel Cerebus neural signal processing system (Blackrock Microsystems). Two different laminar probes were used (U-Probe, Plexon; Vector Array, NeuroNexus). The laminar probes consisted of either 24 or 32 active microelectrodes, linearly spaced 0.1 mm apart, with impedances ranging 0.2–0.8 MΩ at 1 kHz. The probes were connected to the Cerebus amplifier using an analog head stage (Blackrock Microsystems), with the shank of the probe used as the reference. Each recording session, one or two laminar probes were introduced into dorsal V1 through the intact dura mater using a chamber-mounted microdrive (a custom-designed modification of a Narishige International micromanipulator) and adjusted in the z-plane until the majority of microelectrode contacts spanned the entire cortical thickness, from the subdural space to the white matter. Placement of the electrode relative to the cortical laminae was verified using previously established neurophysiological criteria [e.g., CSD profile, local field potential (LFP) correlations, power spectral density], as described below. Gaze position was recorded at 1 kHz (NIDAQ PCI-6229; National Instruments) using an infrared light-sensitive camera and commercially available eye tracking software (EyeLink II, SR Research; iView, SensoMotoric Instruments). All trials where the animal's gaze left the central 1° radius around the fixation spot were excluded from analysis. LFPs were extracted from the broadband signal using a low-pass, fourth-order Butterworth filter with a cutoff frequency of 500 Hz. Single-unit spiking activity was sorted offline using the KiloSort toolbox (Pachitariu et al. 2016) for MATLAB (version R2016b). Visual inspection of the mean and variance of the isolated spike waveforms suggests that KiloSort spike isolation is on par with or even surpasses conventional cluster-based spike sorters (see Pachitariu et al. 2016). We used the KiloSort default parameters for sorting and cluster merging and confirmed that single units did not produce spikes within a 1-ms refractory period.

Laminar alignment. CSD analyses of visual responses to brief visual stimulation have been shown to reliably indicate the location of the primary geniculate input to V1 (to granular layer 4C, or L4) as a distinct current sink that is thought to reflect the initial retinogeniculate volley of activation's combined excitatory postsynaptic potentials (Mitzdorf and Singer 1979; Schroeder et al. 1998). To derive CSD from the LFP, we computed an estimate of the second spatial derivative appropriate for multiple contact points using the following formula (Nicholson and Freeman 1975):

$$CSD(t,c) = \frac{x(t,c-z) + x(t,c+z) - 2x(t,c)}{z^2},$$

where x is the extracellular voltage at time t measured at an electrode contact at position c, and z is the inter-contact distance of the electrode array. The resulting CSD from the formula above was multiplied by 0.4 S/mm as an estimate of the electric conductivity of cortex (Logothetis et al. 2007) to obtain current per unit volume. We restricted our data to measurements within the cortical gray matter by eliminating channels at the top and the bottom of the electrode array that were void of any MUA visual response (see Cox et al. 2019 for details). For display purposes, we created two-dimensional representations of CSD as a function of time and space by interpolating CSD between adjacent electrode contacts, followed by smoothing with a two-dimensional Gaussian filter (s = 0.1 mm and 15 ms) (Pettersen et al. 2006). Microelectrode contacts were determined to be located in the granular layer on the basis of the initial sink of a flash-evoked CSD (see Cox et al. 2019; Cox et al. in press; Dougherty et al. 2017, 2019; Maier et al. 2010; Maier 2013; Ninomiya et al. 2015 for details). Infragranular laminar compartment locations were determined online by the position of the initial sink in response to a flashed stimulus and corroborated by additional neurophysiological criteria such as characteristic patterns of LFP power spectral density (Bastos et al. 2018; van Kerkoerle et al. 2014), signal correlations of the LFP between all channel combinations (Sotero et al. 2015), and the latency (Self et al.

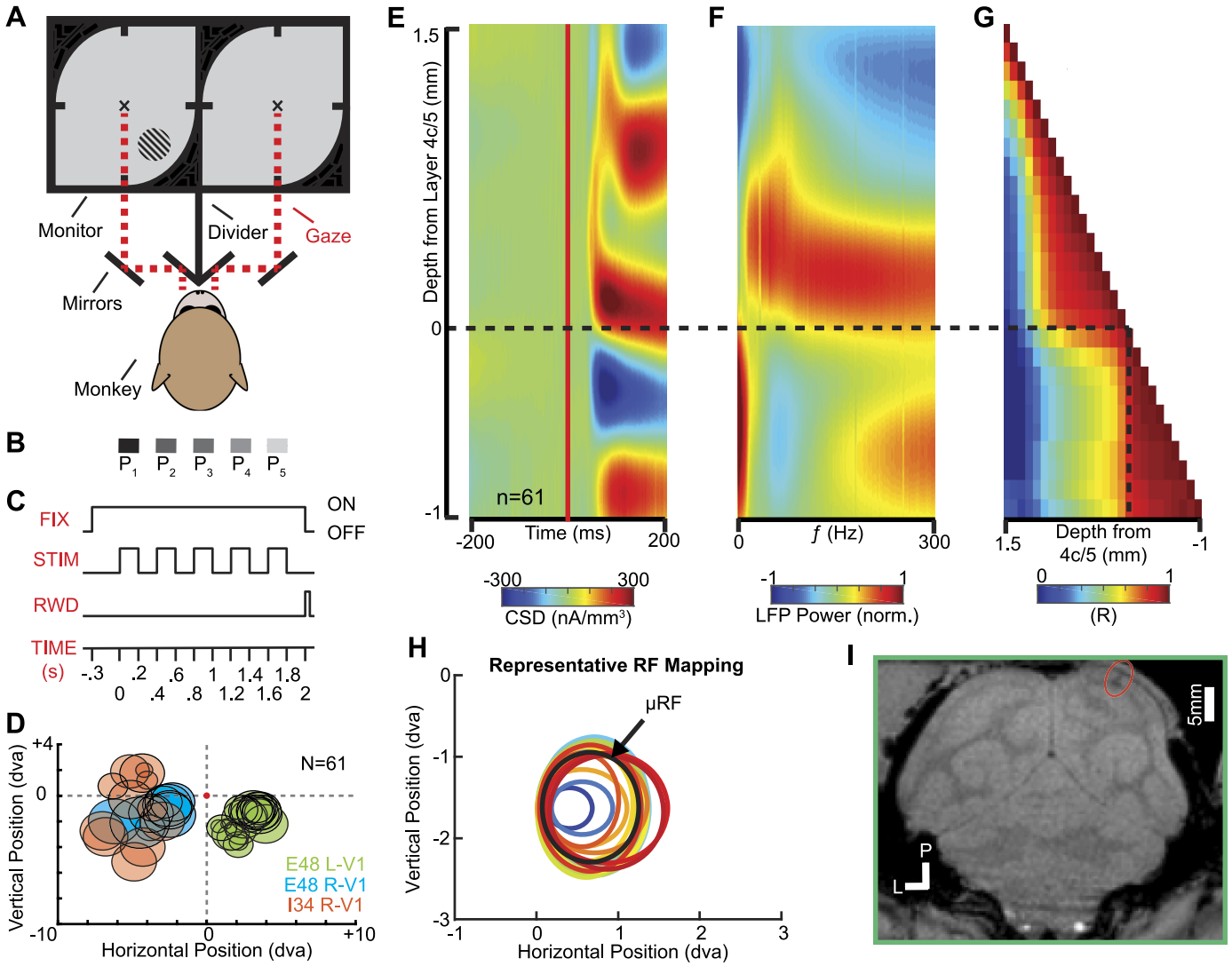

Fig. 1. Experimental setup and paradigm. *A*: diagram of stereoscopic stimulation. Monkeys were positioned behind a set of calibrated cold mirrors such that each eye received stimulation from independent halves of a CRT monitor (see MATERIALS AND METHODS for details). *B*: grayscale to depict each individual presentation (P_1–P_5) of the stimulation sequence. *C*: temporal organization of events in each trial. Each trial consisted of 5 stimuli (STIM) randomly presented to one or both eyes (stimulus parameters detailed in MATERIALS AND METHODS) while the monkeys maintained fixation (FIX). Whenever the monkeys successfully maintained fixation throughout, they received a juice reward (RWD) at the end of the trial. *D*: stimulus sizes (dva, degrees of visual angle) and locations for each recording session (n = 61). Colors encode the animal (E48, I34) and recorded V1 hemisphere (L, left; R, right). *E*–*G*: laminar profiles of stimulus-evoked local field potential (LFP) responses. Ordinate represents cortical depth from the cortical surface toward the white matter, with 0 marking the L4/L5 boundary (dashed line). *E*: average current source density (CSD) profile across both animals and all sessions. Abscissa represents time from stimulus onset (0 ms). *F*: average power spectral density of the V1 LFP across both animals and all sessions (t = 0 to 200 ms). Abscissa represents frequency (f). Power was normalized (norm.) such that at each frequency, the response maximum was set to 1 and the response minimum was set to 0. *G*: average LFP cross-correlations (R) between all electrode-pair combinations following visual stimulation. Abscissa represents cortical depth from the top of cortex (*left*) toward the white matter (*right*). *H*: representative receptive fields (RF) from a single session based on thresholded multiunit activity for each electrode channel. Each color denotes a different channel of the same linear array. Black line indicates the mean RF across all channels. *I*: 7T MRI of neocortex showing the location of an electrode penetration perpendicular to the cortical surface of V1. Red outline highlights the susceptibility artifact caused by cerebrospinal fluid in a tissue track where the electrode was located. L, lateral; P, posterior.

2013) of stimulus-evoked MUA responses (Fig. 1; see Maier et al. 2010 for details). The supragranular to granular boundary was set to 0.5 mm above the granular-to-infragranular boundary.

Receptive field mapping. Once satisfactory electrode placement was achieved, we used a reverse correlation-like technique to map the receptive fields of the single units under study. We first estimated the receptive field location from the audible MUA response to bars and gratings that were moved across the screen while the animals fixated for juice reward. We then had the animals fixate while a series of circular static random noise patches were displayed at pseudorandomized locations within a predetermined virtual grid that covered the estimated receptive field. Up to five stimuli were shown per trial, for 200 ms each with 200-ms blank periods interleaved. Stimulus size and grid spread varied depending on receptive field estimates, with each recording session typically including an initial "coarse" followed by a "fine" mapping phase of decreasing grid size. We used the resulting neurophysiological data to compute retinotopic three-dimensional receptive field matrices (RFMs) (Cox et al. 2013) to derive spatial maps of neuronal responses as a function of visual space. Briefly, for each stimulus presentation, the evoked neuronal response [either MUA or single-unit activity (SUA) from each microelectrode contact] was averaged over time and converted to a z score to produce a single

scalar value for each trial. The portion of virtual grid corresponding to the stimulus location was then filled with that value, producing a three-dimensional matrix consisting of one dimension for vertical visual space, one dimension for horizontal visual space, and one dimension for stimulus presentations. The third dimension was then collapsed via averaging, producing a spatial map of each unit's retinotopic response. Sessions where receptive fields did not overlap across all electrode channels were eliminated from analysis.

To optimally stimulate isolated neurons, we followed the receptive field mapping procedure by an automatized estimation of size and spatial frequency tuning. This procedure resembled the receptive field mapping paradigm, in that five stimuli were presented in sequence while the monkeys fixated. However, instead of changing the position of the stimuli, we kept them constant, centered over the previously established receptive field area, while we randomly varied the size or spatial frequency of each of the presented gratings. The data were then analyzed using custom-written MATLAB scripts. The stimulus size and spatial frequency that evoked the maximal response were then used in the task described in *Behavioral task and visual stimulation.*

Analysis of single-unit spiking activity. All analyses of SUA were performed using custom-written scripts in MATLAB. Trials with exceeding electrical noise or motion artifacts were excluded using the generalized extreme studentized deviate (ESD) correction (Rosner 1983) at the unit level by computing

$$R_i = \frac{max_i\left[x_i - \bar{x}\right]}{s}$$

and

$$\lambda_i = \frac{(n-i)t_{p,n-i-1}}{\sqrt{(n-i-1+t^2_{p,n-i-1})(n-i-1)}} i = 1, 2, \ldots, r,$$

where the number of outliers for a given unit is the largest i, up to a preset maximum number of outliers r, such that R_i, the computed extreme studentized deviate, is larger than the computed critical value, λ_i, n is the number of trials, s is the standard deviation of the maximum values of each trial, x is the maximum value of the trial, $t_{p,v}$ is the value of the t distribution with v degrees of freedom ($\alpha = 0.05$), and

$$p = 1 - \frac{\alpha}{2(n-i+1)}.$$

Spiking data were convolved using a Poisson distribution resembling a postsynaptic potential, because that has been shown to be a useful estimation of the downstream effect of a single-unit's spiking activity (Thompson et al. 1996). Spike rate (R) is computed at time t where

$$R(t) = \left[1 - \exp\left(-\frac{t}{\tau_g}\right)\right] \times \left[\exp\left(-\frac{t}{\tau_d}\right)\right]$$

such that τ_g and τ_d are the time constants for growth and decay, respectively. Data from previous studies suggest values of 1 and 20 ms as valid for τ_g and τ_d, respectively (Kim and Connors 1993; Mason et al. 1991; Sayer et al. 1990; Thomson et al. 1993a, 1993b).

For investigation of within-unit conditional changes (e.g., initial to repetition conditions), the convolved spiking data was analyzed using a receiver operating characteristic (ROC) (Green and Swets 1966). Conditional differences were quantified by taking the average spiking rate of each unit between 40 ms post-stimulus onset to stimulus offset for each repetition. These average values then served as the parameter λ to generate Poisson processes across values k of the distribution:

$$F(k, \lambda) = \frac{\lambda^k e^{-\lambda}}{k!}.$$

For each condition, k values from the Poisson distributions were used to generate ROC curves, where k was the number of trials for whichever of the two conditions in which we recorded fewer trials. The area under the curve (AUC) of the ROC curve, sampled at 100 points equally spaced between the minimum and maximum values taken from the Poisson distributions, was then compared with AUC values derived from random Poisson distributions whose λ values were randomized averages chosen from a combined sample that consisted of both conditions. This procedure was bootstrapped 1,000 times to determine whether the difference between the conditions was significant. Significance was reached if the original value of the area under the ROC curve was outside the 95% confidence interval of the bootstrapped values.

Units with no significant response to visual stimulation, determined by performing a paired-samples t-test ($\alpha = 0.05$) on the mean baseline activity on each trial and the mean activity during the epoch of visual stimulation (40 ms post-stimulus onset to stimulus offset), were excluded from analysis. Additionally, units whose average maximum firing rate in response to visual stimulation did not exceed 5 spikes/s were excluded from analysis.

SUA was made comparable across individual units with differing average spike rates by normalizing their responses at the unit level:

$$z_t = \frac{x_t - \text{mean}(x_b)}{\max(x) - \text{mean}(x_b)},$$

where x_t is the averaged data for all stimulus orientations in each set at time t and x_b is the averaged data restricted to the baseline epoch. The baseline epoch was defined as the 100-ms interval of passive fixation leading to the onset of the stimulus. The maximum response was defined as the maximum value that a single unit achieved across all presentations during the stimulation epoch. z_t is the resultant normalized value at time point t.

Statistical tests were performed at the unit level using two-tailed, paired-samples t-tests ($\alpha = 0.05$) and adjusted using the Benjamini-Hochberg procedure for false discovery rate (FDR) at $\alpha = 0.05$ (Benjamini and Hochberg 1995).

To determine the latency of neuronal responses, each unit was tested by computing paired-samples t-tests ($\alpha = 0.05$) of the convolved neural signal at each recorded time point against the baseline (prestimulation) epoch on each trial. The point at which the response deviated significantly from the baseline for five sequential samples was found to be the latency of that response. The mean latency was taken for each unit. The mean of these values for all units was taken to obtain the population average.

Tests for ocularity. We used a custom-designed mirror stereoscope (see Cox et al. 2019; Cox et al. in press; Dougherty et al. 2019) to evoke neuronal responses specific to each eye. For any given stimulus presentation, the stimulus could be presented to either the left eye or the right eye, or to both eyes simultaneously. We used the neuronal responses to monocular stimulation to compute an ocularity index for each unit that quantifies their selectivity for one versus the other eye. Similarly to recent work on ocular dominance in V1 (Romero et al. 2007; Zhang et al. 2005), we computed a quantitative ocularity index (OCI) using a Michelson contrast (Michelson 1927) to compare single-unit responses between stimulus presentations to the left and right eyes:

$$OCI_i = \left| \frac{\text{mean}(x_{i,L}) - \text{mean}(x_{i,R})}{\text{mean}(x_{i,L}) + \text{mean}(x_{i,R})} \right|,$$

where the ocularity index for unit i (OCI_i)was defined as the absolute value of the difference between the mean response x for unit i on trials where the stimulus was monocularly presented to the left eye ($x_{i,L}$) and when the stimulus was presented monocularly to the right eye ($x_{i,R}$), divided by the sum of those two responses.

To derive the average stimulus responses, we computed the mean spike rate between 40 ms post-stimulus onset to stimulus offset. We defined units with an OCI >0.6 as "monocular" units, whereas units with an OCI <0.4 were defined as "binocular" units.

Anatomical MRI. Animals were anesthetized using the same procedure as outlined under *Animal care and surgical procedures*. Anesthetized animals were then placed inside a Philips Achieva 7T MRI scanner (Koninklijke Philips) at the Vanderbilt University Institute of Imaging Science and remained anesthetized throughout the duration of the scan. Vital signs were monitored continuously. T1-weighted three-dimensional MPRAGE scans were acquired with a 32-channel head coil equipped for SENSE imaging. Images were acquired using a 0.5-mm isotropic voxel resolution with the following parameters: repetition time 5 s, echo time 2.5 ms, and flip angle 7°.

RESULTS

Adaptation of neural circuits is an area of active research (Kar and Krekelberg 2016; Quiroga et al. 2016). We were curious about the general effect of repetition-induced sensory adaptation on the primate primary visual pathway. Specifically, we were eager to determine the primary site of cortical adaptation within the columnar microcircuit of visual cortex. We devised a stimulation sequence consisting of five consecutive stimulus repetitions where stimulus location and size was held constant while stimulus identity was variable. Each stimulus consisted of a static sine-wave grating of fixed contrast, phase, and spatial frequency, but varying orientation. Each grating was presented for 200 ms, followed by a 200-ms ISI (Fig. 1, *A–D*). Two monkeys were trained to perform this task ($N = 48$ sessions in *monkey E48*, $N = 13$ in *monkey I34*). Following successful cortical penetration with a linear multielectrode array and careful laminar alignment (see MATERIALS AND METHODS and Fig. 1, *E–I*), we recorded visual responses across all layers. Visual stimuli always spanned the combined receptive fields of the recorded neurons (see MATERIALS AND METHODS).

V1 spiking suppression during repetitive visual stimulation. We first characterized the adaption-related changes of spiking activity across V1 layers. Across all recording sessions in both animals, we collected the responses of 278 single units (see MATERIALS AND METHODS). We sampled units from the upper (supragranular, $n = 110$), middle (granular layer, 4C $n = 112$), and lower (infragranular, $n = 56$) layers.

We first examined laminar SUA across consecutive stimulus presentations, irrespective of stimulus orientation or stimulated eye (see below for a detailed analysis of each of these parameters in isolation). This comparison revealed a general response reduction to repeated visual stimuli across all V1 layers, which affected both the initial transient as well as the sustained phase of the visual response (Fig. 2). The largest repetition-induced decrease in spiking occurred immediately following the first stimulus repetition, with smaller spike rate decrements for subsequent presentations (see Fig. 2*D* for statistics).

Collapsing the neuronal population responses across time, we found that all stimulus repetitions evoked significantly

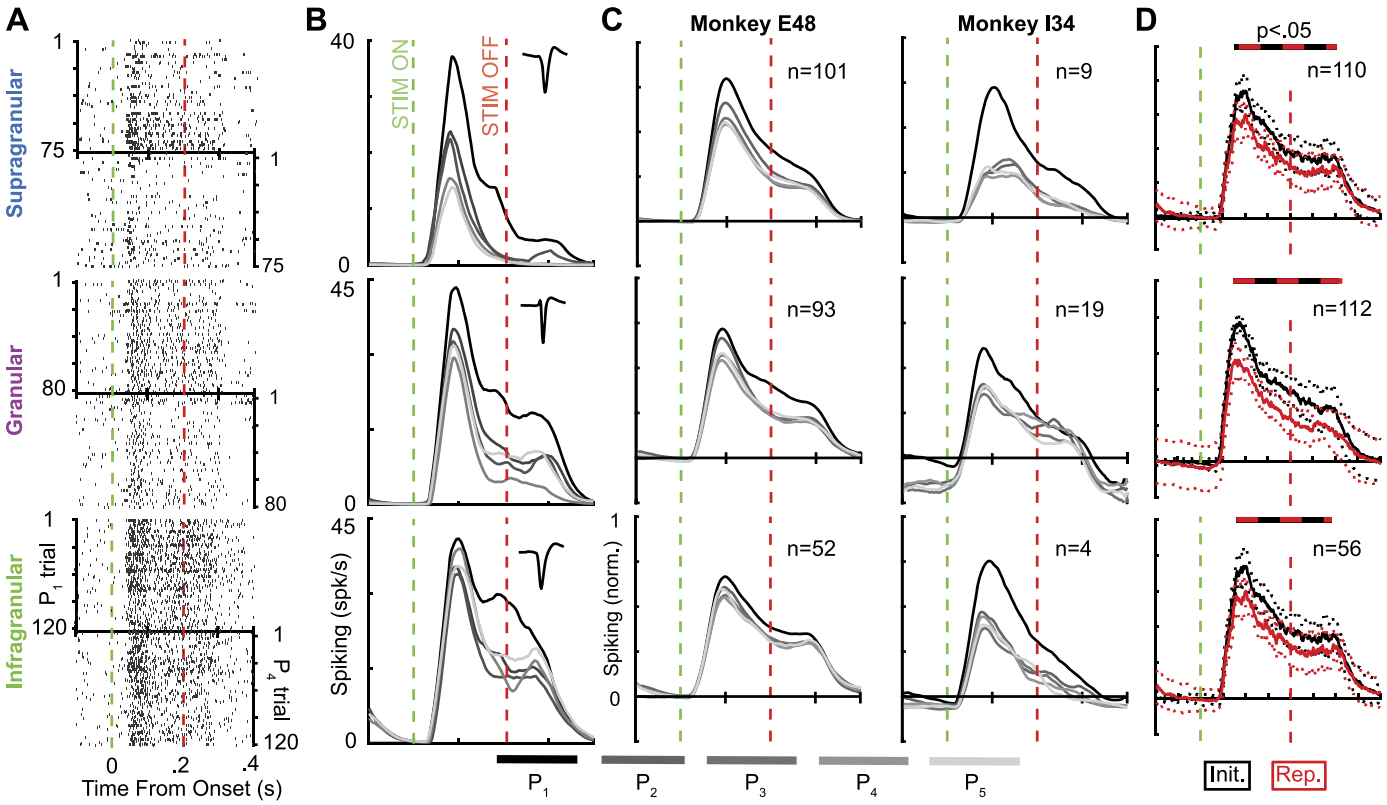

Fig. 2. V1 single-unit responses. *A*: raster plots of representative single-unit responses for each of the 3 main laminar compartments (indicated at *left*) for the first (*top*) and fourth (bottom) presentations of each sequence. Green vertical lines indicate the onset of the visual stimulus (STIM ON). Red lines represent stimulus offset (STIM OFF). *B*: spike density functions for the same responses as in *A*. The response to each presentation is denoted by grayscale, with black indicating the first (P_1) and the lightest gray indicating the fifth presentation (P_5) of each sequence (*bottom*). *Insets* represent the mean spiking waveforms for each respective unit. *C*: median spike density functions for each monkey across all normalized single-unit responses per laminar compartment (n = no. of units). *D*: representation of median single-unit response profiles across both monkeys for each of the main laminar compartments. Black solid line is the median response for P_1 in the sequence (Init.). Red solid line is the response to P_4 (Rep.). Dotted lines represent the 95% confidence interval (CI) for the response with the corresponding color. Black and red bar above each plot denotes when P_1 and P_4 responses were significantly different at each time point after stimulus onset using paired-samples t-tests ($P < 0.05$).

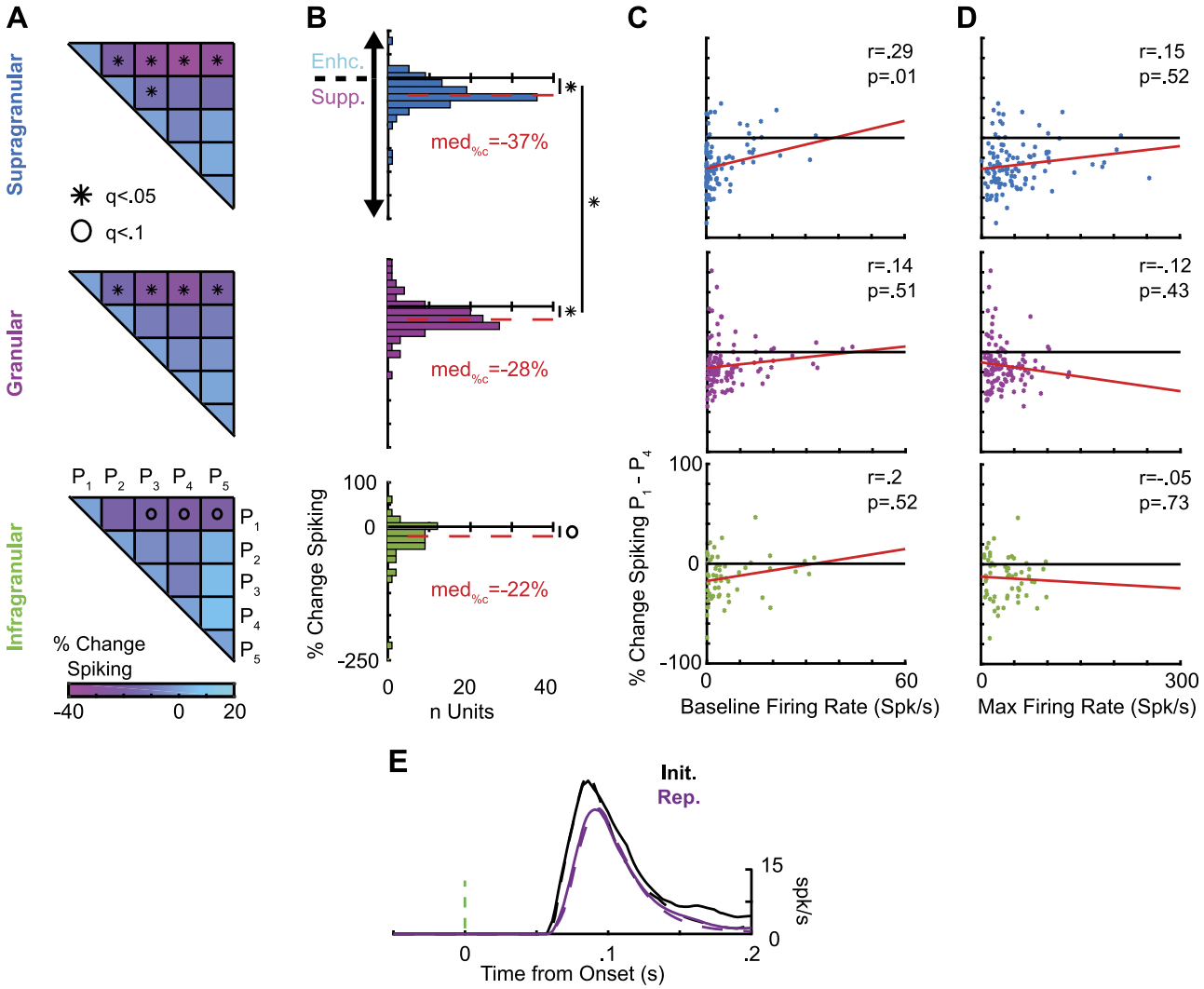

Fig. 3. Laminar profile of V1 repetition-induced spiking suppression. *A*: change in population response between each subsequent stimulus presentation P_1–P_5. Color represents percent change of evoked spiking. Laminar compartment is denoted at *left*. *$q < 0.05$, significant differences (see MATERIALS AND METHODS); ○$q < 0.1$, differences approaching significance. *B*: distribution of single-unit response differences in percent change between P_1 and P_4. Values <0 denote response suppression. Median response ($Med_{\%c}$) is indicated by a red dashed line. Enhc., enhancement; Supp., suppression. *C*: correlation of each unit's average baseline firing rate with its spiking difference between P_1 and P_4 (spk/s, spikes/s). Baseline firing was defined as the average firing rate during 100 ms of fixation immediately before the first stimulus presentation. Laminar compartment is indicated by color. No significant correlation ($P < 0.05$) was found for the majority of laminar compartments, with the exception of supragranular layers. *D*: correlation of response change between P_1 and P_4 and average maximum firing rate for each unit during the stimulation epoch (40 ms post onset to offset). No significant correlation was found for any laminar compartment. *E*: median spike density function (SDF) of an example unit before (solid lines) and after (dashed lines) elimination of trials contaminated with microsaccades. Black lines are the SDF for P_1 (Init.), and purple lines are the SDF for P_4 (Rep.). A paired-samples *t*-test revealed no significant difference between the two SDFs.

smaller responses than the initial presentation in both granular layer and supragranular layers (Fig. 3). Repetition-induced spiking decreases were also observed in the infragranular layers, where they approached significance (Fig. 3, *A* and *B*; paired-samples *t*-test, corrected with FDR at $\alpha = 0.05$). Comparing population responses for the second through fourth presentations using the same technique, we found significant differences between the second and third presentations in the supragranular layers only (Fig. 3*A*, *top*). These results suggest that although generalized adaptation to repeated stimuli affects neurons across all layers of V1, it is most pronounced in the superficial layers and remains more or less constant after stimuli have been repeated one or two times.

As a next step, we moved beyond the level of population averages and compared each recorded neuron's response between the initial and the fourth presentations. This analysis revealed that the majority of neurons in all layers exhibited repetition suppression (Fig. 3*B*). Statistical comparison revealed that the median magnitude of suppression for neurons in the supragranular layers was significantly larger than that in granular layer 4C (paired-samples *t*-test, $\alpha = 0.05$), whereas suppression for all other laminar comparisons was not significant. The magnitude of this repetition suppression was largely independent of individual differences in baseline or maximum firing rates (Fig. 3, *C* and *D*) and also was not affected by microsaccade rate (Fig. 3*E*).

Last, we tested for statistical significance of repetition suppression on the single-neuron level by comparing the observed responses to artificially created Poisson-distributed random spike trains (see MATERIALS AND METHODS). This approach pro-

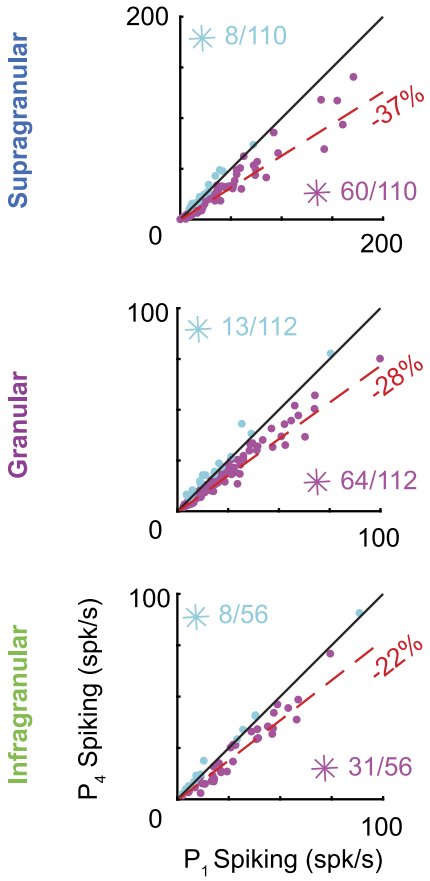

Fig. 4. Statistical comparison of repetition-induced response differences using Poisson spike train analysis (see MATERIALS AND METHODS). Each single unit is represented by a dot in a scatter plot where the median spiking response to the first presentation (P_1) is compared with that of the fourth (P_4). Magenta asterisks denote number of units showing significant response suppression in each compartment. Cyan asterisks denote the number of single units with significant response facilitation. Spk/s, spikes/s.

vides a more accurate estimate of observed spike rate differences than statistical techniques based on normal distributions (Thompson et al. 1996). We found that, across all laminar compartments, the majority of neurons showed a significant decrease in spiking, with a handful of neurons showing significant spiking increases when the stimulus was repeated (Fig. 4).

Importantly, extending the stimulation period from 200 to 500 ms (while keeping the ISI constant at 200 ms) yielded a qualitatively similar pattern of repetition suppression across V1 layers (Fig. 5). This result suggests that the spiking suppression described above is not specific to the timing parameters of our main paradigm but applies to stimulus repetitions more generally.

Current source density indicates reduced synaptic activity during repeated stimulation. As described above, the laminar profile of single-unit spiking revealed that the layers harboring the bulk of cortico-cortical connections (supragranular V1) showed the greatest effect of adaptation. Although this finding hints at a supragranular origin of cortical adaptation, evaluation of synaptic currents is necessary to understand exactly where these changes initially take place. Therefore, we next computed the laminar CSD, which provides a quantitative measure of volume-averaged transsynaptic current flow in the form of spatially circumscribed current sinks and sources (Mitzdorf 1985; Schroeder et al. 1998). In general, current sinks are linked to net depolarization, whereas current sources are linked to passive return currents (Mitzdorf 1987).

Figure 6 shows the grand average laminar CSD as a function of time across all stimulus repetitions. The initial current sink in V1 granular layer 4C following onset of visual stimulation is indicative of retinogeniculate synaptic activation (Godlove et al. 2014; Maier 2013; Mitzdorf 1987; Schroeder et al. 1998; van Kerkoerle et al. 2014). The subsequent current sinks in extragranular layers are believed to reflect net depolarization due to cortico-cortical processing (Cox et al. 2019; Douglas et al. 1988; van Kerkoerle et al. 2014). Current sources are also shown in Fig. 6. Comparison of the laminar CSD profile for the first 25 trials (Fig. 6, *left*) with the average CSD profile for the last 25 trials of each experiment (*middle*) reveals that the location of the sinks remained constant, suggesting that there was little to no electrode movement over the course of the experiment. Confirming that there was no relative movement of the electrode and the neural tissue is important because it allows us to directly compare the magnitude of CSD responses between stimulation conditions.

Figure 7*A* shows the average CSD response to each stimulus repetition for the supragranular, granular, and infragranular

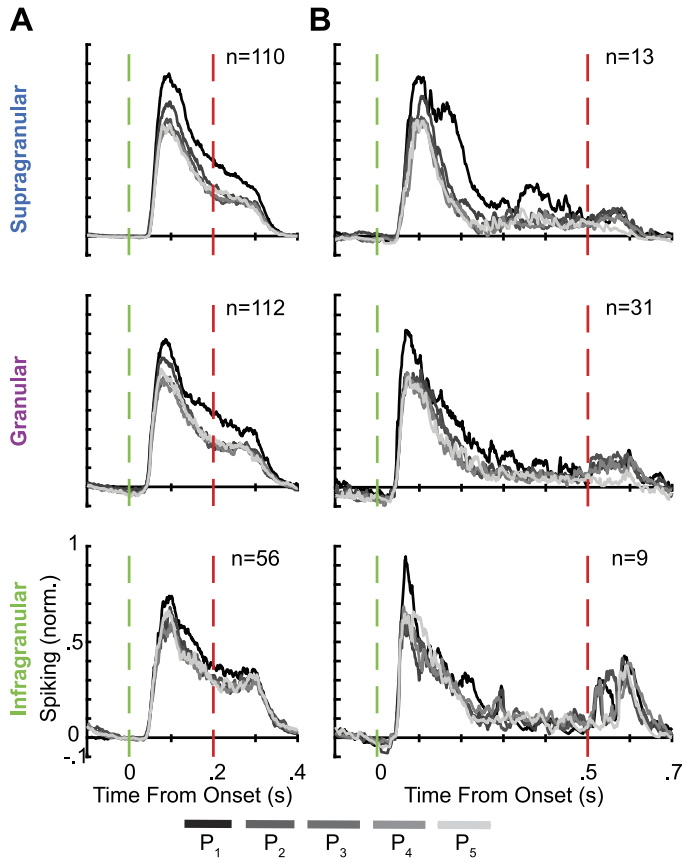

Fig. 5. Repetition suppression following longer stimulation epochs. *A*: median normalized response for both monkeys across presentations (P_1–P_5; key at *bottom*) for the 200-ms stimulation condition shown in Fig. 2, without smoothing. Green vertical dashed line denotes stimulus onset; red vertical dashed line denotes offset. *B*: spike density functions for a control experiment using the same paradigm in *A* with a stimulus duration of 500 ms followed by a 200-ms interstimulus interval ($N = 10$ sessions in *monkey I34*; n = no. of units).

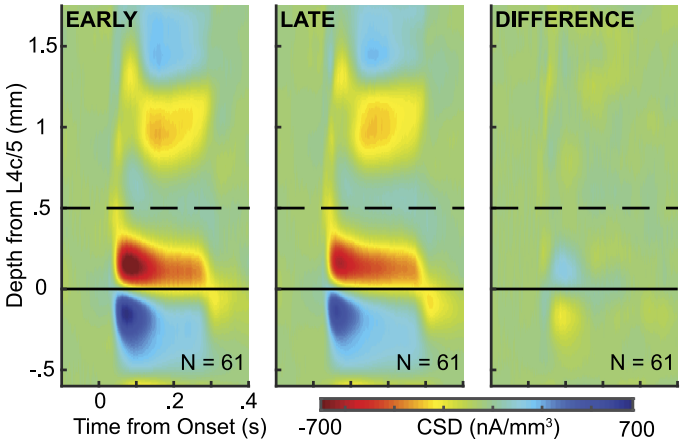

Fig. 6. Comparison of laminar current source density (CSD) profiles across the depth of cortex between early in the recording session (first 25 stimulus presentations; *left*) and late in the session (last 25 stimulus presentations; middle), averaged across all sessions. The dashed line denotes the boundary of layer 4/5 (L4/5). Subtraction (*right*) suggests that there was little movement in the positioning of the linear microelectrode array throughout the session.

layers, respectively. For ease of comparison, current sinks are plotted as positive deflections and current sources as negative deflections. Matching the overall profile of the stimulus-evoked CSD discussed above, the granular and supragranular layers (Fig. 7*A*, *top* and *middle*) exhibited a net current sink, whereas the infragranular layers showed a net current source (bottom). The initial stimulus presentation of each sequence evoked a larger CSD response than all ensuing repetitions, suggesting decreased synaptic activation to repeated stimuli. Interestingly, this relative difference in response magnitude was most pronounced in the supragranular layers, suggesting that the largest adaptation of the synaptic response occurred after the feedforward, retinogeniculate activation of layer 4C. The response in the infragranular layers is of diminished interpretative value because it is dominated by return currents that are passive in nature.

Another interesting aspect of the CSD adaptation shown in Fig. 7 is the temporal variance between laminar compartments. To further investigate these temporal differences, we subtracted the layer-specific CSD response for the fourth stimulus presentation from that of the initial stimulus presentations (Fig. 7*B*). As expected, this subtraction showed that the largest difference in net depolarization was located in the supragranular layers. Interestingly, the temporal dynamics of this CSD adaptation is initially identical for the granular and supragranular layers, suggesting that there is a certain diminishment in the initial (granular) synaptic activation during stimulus repetitions that gets further amplified in the supragranular layers. It is noteworthy that feedback projections to the extragranular layers, even those targeting local interneurons, are excitatory and thus associated with increased synaptic activity rather than decreased net depolarization.

We next compared the laminar evolution of spiking responses to the laminar evolution of CSD (Fig. 8). Inspection of the full response sequence reveals that both the overall spiking (Fig. 8*A*) and overall CSD responses (Fig. 8*B*) are largest for the initial stimulus presentation and smaller for all stimulus repetitions. Interestingly, the smallest CSD response occurred for the second stimulus, which is coincident with the biggest differential in spiking (Fig. 2). However, in contrast to the spiking response, the CSD magnitude increased again slightly for ensuing repetitions (while staying below the initial response). This difference between the temporal evolution of laminar CSD and laminar spiking seems to suggest some form of divergence, or uncoupling, between local synaptic activation and generated spiking. However, it is important to keep in mind that CSD is a complex population signal that needs to be interpreted with care (see also Gratiy et al. 2017; Halnes et al. 2017).

Contrasting the change in population spiking (Fig. 8*C*) and CSD (Fig. 8*D*) between the initial stimulus and a repeated stimulus revealed another interesting pattern. Most neurons exhibiting an early onset of adaptation were located within the

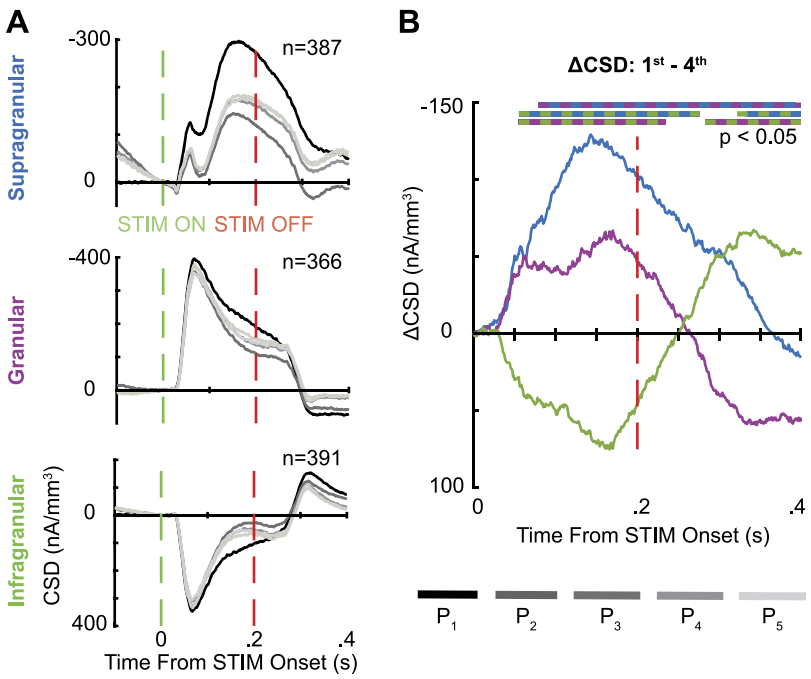

Fig. 7. *A*: stimulus-evoked current source density (CSD) response for each laminar compartment, averaged across all respective channels and across sessions (n = no. of units). Green dashed line denotes stimulus onset (STIM ON), and red dashed line denotes offset (STIM OFF). Current sinks are plotted upward (i.e., as positive values). Laminar compartments are denoted at *left*. Repetition numbers are indicated in gray-scale (*bottom right*). *B*: subtraction plot of CSD activation between the first and fourth presentations (ΔCSD; average of all channel-based subtractions). Significant differences between laminar compartments across time are indicated by color-coded horizontal bars (paired-samples t-test, $P < 0.05$). Stimulus repetitions yielded a similar pattern of laminar CSD as the initial presentation; however, both sinks and sources were reduced for repeated stimuli compared with the initial response. This finding suggests that the diminished spiking responses under repetitive stimulation are secondary to decreased synaptic drive.

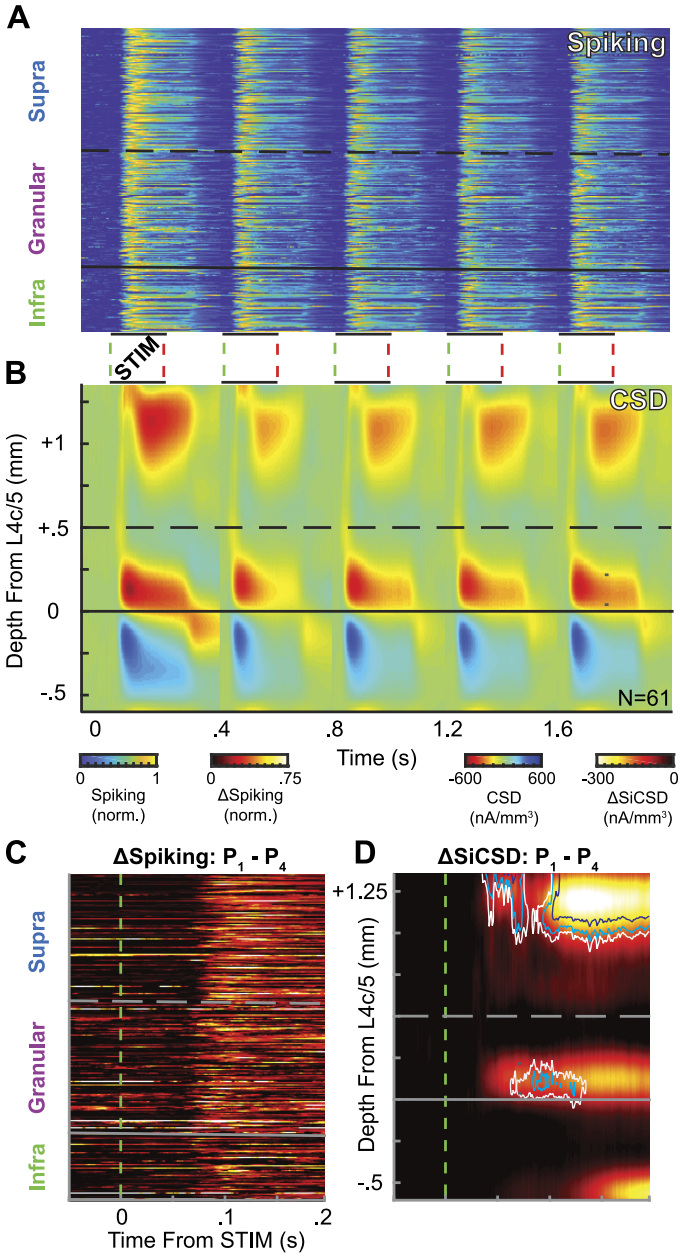

Fig. 8. Laminar profile of evoked responses for the entire stimulus sequence. *A*: single-unit spiking responses, organized by laminar compartment. Each row indicates the spiking responses of 1 unit across the entire trial (i.e., all 5 stimulus subsequent presentations), averaged across all trials. Periods of visual stimulation (STIM) are denoted by horizontal bars at *bottom*. All single-unit responses were normalized (norm.) for comparison (see MATERIALS AND METHODS). *B*: mean current source density (CSD) across presentations. Stimulation is denoted by bars at *top*. *C*: difference in laminar spiking (ΔSpiking) between first (P_1) and fourth (P_4) stimulus presentations, averaged across sessions. *D*: difference in CSD sinks (ΔSiCSD) between P_1 and P_4, averaged across sessions. Interior of navy outline denotes $P < 0.01$; light blue outline, $P < 0.05$, and white outline, $P < 0.1$. Note that targeted feedback to inhibitory interneurons should result in a net increase of synaptic activity and thus an increase in CSD. The net decrease in current sinks shown suggests that the repetition-induced adaptation of synaptic drive in V1 might be supported by a different mechanism.

granular layers, although individual neurons showed variable degrees of adaptation across layers (Fig. 8*C*). In contrast, both the earliest and largest CSD adaptations were localized in the supragranular layers (Fig. 8*D*). This laminar differential in current flow suggests that the majority of the adaption-related decrease in synaptic drive occurs outside V1's primary input layer. Indeed, the reduction of CSD magnitude in granular layer 4C did not reach significance until after significant supragranular adaptation (see Fig. 8*D*).

Quantitative differentiation of these laminar temporal dynamics was achieved by calculating the relative adaptation onset times (or "latencies") for both the population spiking and localized current sinks (Fig. 9). In line with the causal relationship between synaptic depolarization and spiking activity, we found that the onset latency of current sinks (SiCSD) generally preceded that of spiking activity (Fig. 9*A*). Note that the infragranular layers were dominated by a passive current source, which precludes them from this analysis. This comparison confirmed that the granular layers generally exhibit a current sink ahead of the supragranular layers, which is explained by the fact that the granular layers receive the bulk of V1 inputs (Douglas and Martin 1991).

We were especially curious about comparing the onset of adaptation-related differences in CSD and spiking across layers (Fig. 9*B*). Because the granular layers receive the vast majority of sensory inputs whereas extragranular layers are dominated by cortico-cortical projections, any differences in the temporal onset of adaptation between these compartments could be indicative of thalamocortical or intracortical processes, respectively. We found that visually evoked current sinks in the supragranular layers showed the first significant reduction during stimulus repetition. This supragranular reduction in net depolarization was followed by reduced spiking. Reduction of net depolarization in the granular layers occurred only after both the current sink in the upper layers and spiking throughout the whole cortical column showed significant adaptation (Fig. 9*B*). These findings, taken together, suggest that the majority of repetition-related reductions in synaptic drive cannot be explained by reduced sensory input to V1 alone. Instead, the bulk of repetition suppression in V1 arises from reduced intracortical signaling during interlaminar propagation of sensory activation.

Interocular transfer of response suppression. Because the CSD analyses described above implicated an intracortical origin of V1 repetition suppression, we performed another analysis to confirm the result. To do so, we alternated repeated stimulation between the two eyes. This paradigm is revealing because the two retinae receive no feedback from their projection targets in the primary visual pathway (Ortiz et al. 2017). At the next step of visual processing, the lateral geniculate nucleus (LGN), almost all neurons respond to one eye only (Zeater et al. 2015). Hence, sensory signals from the two eyes remain largely segregated before they arrive in V1. We thus reasoned that finding a similar pattern of repetition suppression following interocular stimulus alternation would provide further evidence of an exclusively intracortical origin. In the same vein, if repetition-related response reductions were mostly due to sensory adaptation at earlier (i.e., monocular) stages of visual processing, V1 repetition suppression should be significantly reduced when stimulation alternated between the two eyes.

To perform this analysis, we divided our sample into units that were strongly biased toward one eye (monocular neurons) and units that responded to both eyes similarly (binocular neurons) (see MATERIALS AND METHODS). The majority of monocular neurons were located in the granular layers (20/37 single

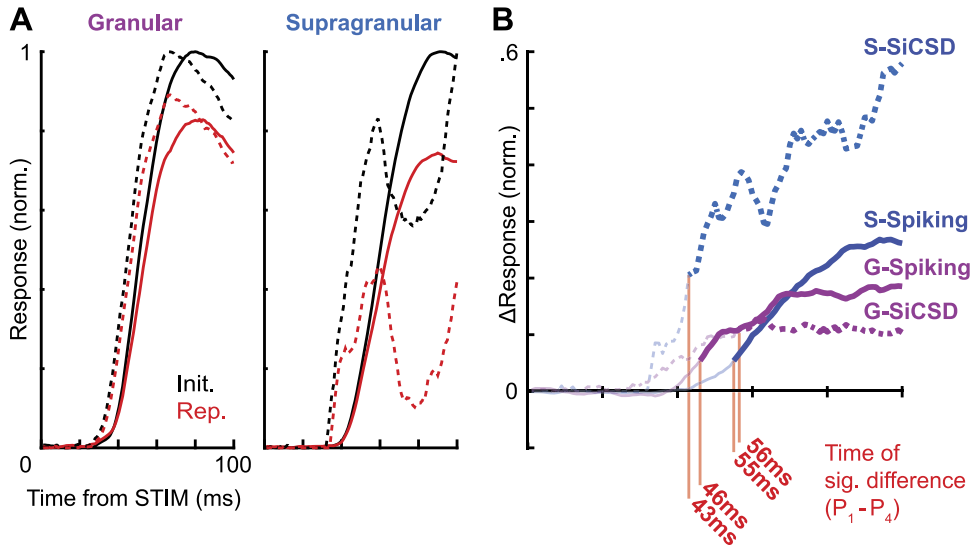

Fig. 9. Temporal evolution of laminar activation. *A*: initial transient spiking (solid lines) and current source density sink (SiCSD; dashed lines) responses to the first (Init.; black) and fourth (Rep.; red) stimulus presentations for the granular and supragranular laminar compartments. Each response was averaged across all sessions ($N = 61$) and both monkeys. Responses were normalized between the baseline and maximum response for comparison. *B*: subtractive analysis between conditions where the response to the fourth presentation (P_4) is subtracted from first (P_1) for each data type-compartment combination. Color denotes laminar compartment (blue, supragranular; purple, granular), and lines denote spiking (solid) or SiCSD (dashed). Red drop lines show when the difference between conditions becomes significant through a *t*-test at each data point with a *P* value <0.001 for more than 10 consecutive samples. Supragranular SiCSD differences precede spiking differences in both laminar compartments, and granular SiCSD does not become significantly different until after spiking has already been suppressed.

units), whereas the remainder were found across the infragranular and supragranular layers. A more detailed analysis of the laminar distribution of ocularity-dependent responses is reported elsewhere (Dougherty et al. 2019). We first determined that these ocular preferences did not differ significantly between stimulus repetitions (Fig. 10*A*). We then compared the visual responses of each neuronal population across two conditions (Fig. 10*B*). In the first condition, the initial stimulus was presented to the same eye as the repeating stimulus. In the second condition, the initial stimulus was shown to the neurons' dominant eye while the repeating stimulus was shown to the other eye. Our rationale for this analysis was that because of their monocular nature, neurons in the retina or the LGN would be insensitive to the stimulus repetition if adaptation occurred in the other eye. Only neurons that received inputs from both eyes (binocular neurons) were expected to exhibit repetition suppression if stimulus repetition was limited to the eye that was not initially stimulated.

We found that monocular V1 neurons showed no significant reduction of activity when the initial stimulus was shown to one eye and the repeating stimulus to the other eye. In contrast, binocular V1 neurons showed significant repetition suppression independently of ocular configuration (Fig. 11). Because binocular neurons constituted 84% of our sample, it follows that the vast majority of V1 neurons show repetition suppression independently of whether the same or opposite eyes underwent stimulus repetition. This finding suggests that V1 repetition suppression occurs even in the absence of sensory adaptation of monocular neurons in the retinas and the LGN, which further supports the notion of a cortical origin of repetition-related adaptation.

DISCUSSION

The reduced spike rates to repeated visual presentations observed in our study mirror earlier findings in early visual cortex of anesthetized cats (Albrecht et al. 1984; Movshon and Lennie 1979; Summerfield et al. 2008), rodents (King et al. 2016), and monkeys (Hansen and Dragoi 2011). However, this study is the first to our knowledge demonstrating that stimulus repetition modulates the sequential pattern of synaptic activation along the canonical cortical microcircuit (Douglas and Martin, 1991), suggesting that adaptation predominantly affects intracortical processing of sensory signals. This notion was further supported by our finding that V1 repetition suppression survives stimulus manipulations that reduce adaptation in the sensory periphery.

Putative mechanisms. The most striking response difference caused by stimulus repetition was a diminished current sink in the supragranular layers (Fig. 12). Whether the origin of this reduced synaptic response originates in V1 or is fed back from downstream stages of the visuocortical hierarchy cannot be determined from the laminar pattern of CSD alone. It is also conceivable that the visual pulvinar, which projects to V1's uppermost layer (Benevento and Rezak 1976; Kaas and Lyon 2007; Ogren and Hendrickson 1977; Rezak and Benevento 1979), supports adaptive processing; however, we are not aware of any neurophysiological studies demonstrating visual adaptation in the pulvinar. Single-unit recordings in the pulvinar are needed to shed light on this possibility.

Previous studies found that repetitive stimulation of the same retina evokes reduced visual responses (Baccus and Meister 2002; Berry et al. 1999; Victor 1987). Yet, the repetition-related difference in initial synaptic activation in granular layer 4C was too small to reach significance in our sample. Therefore, the cortico-cortical reduction observed either occurs independently of, or strongly amplifies, any such small decrement in initial sensory activation. This interpretation is consistent with earlier work in anesthetized macaques and rodents, showing weaker visual adaptation in LGN compared with V1 (King et al. 2016; Kohn 2007). Anatomically, it is also possible

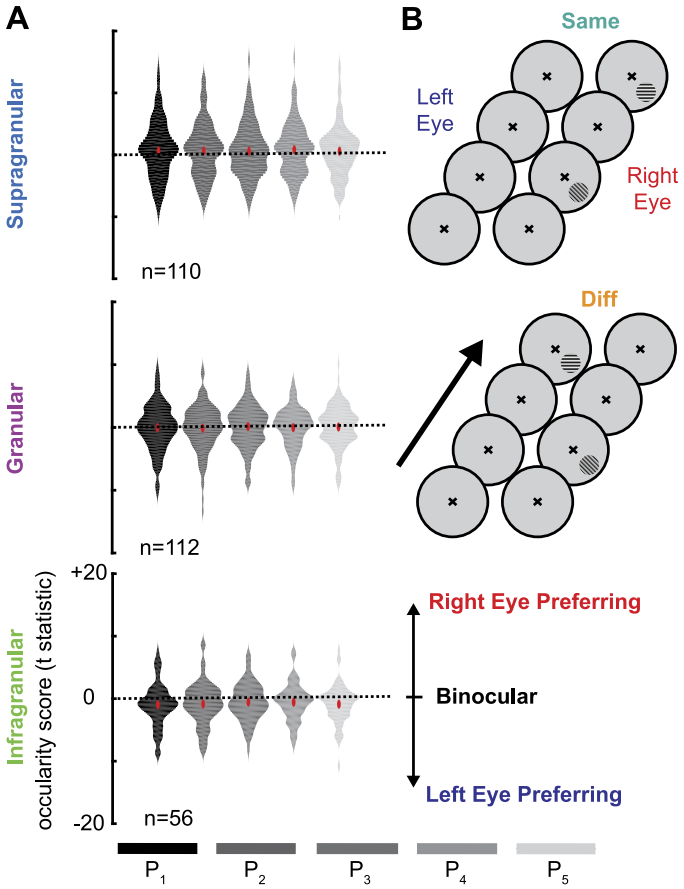

Fig. 10. *A*: ocularity across laminar compartments (denoted at *left*), shown as violin plots as a function of presentation number (P_1–P_5; *bottom*) (n = no. of units). *B*: visualization of the conditions of interest for the ocularity analyses. The initial stimulus was presented to the same eye (*top*) or the other eye (Diff; *middle*) from the repeating stimulus. Binocular units responded to both eyes similarly (*bottom*). Arrow at *middle* depicts the order of sequence (see MATERIALS AND METHODS for timing information and further details).

that LGN neurons inherit some aspects of repetition suppression via corticofugal feedback from V1. However, optogenetic inactivation of rodent V1 does not abolish sensory adaptation in the LGN (King et al. 2016).

Temporal evolution of laminar activation. One of the most compelling findings of this study stems from the direct comparison of the temporal evolution of repetition-related differences in current sinks and population spiking within the cortical column. This analytic approach gains explanatory strength when it is applied to the granular and extragranular laminar compartments because these layers are predominantly associated with bottom-up/feedforward and top-down/feedback processing, respectively.

Our finding that the initial repetition-induced reduction in activity occurs in the uppermost layers of cortex is in line with the notion of a predominantly cortical origin of visual adaptation. It is possible, however, that the underlying process is more complex, because spiking responses in the granular layers were the first to be significantly reduced on stimulus repetition. One possible explanation for this peculiar laminar pattern of activation might be that it is mostly caused by granular neurons whose dendrites span into the supragranular layers. Another possibility is that repeated stimulation disproportionally affects koniocellular neurons of the LGN, which provide inputs to the supragranular layers of V1 (Casagrande 1994; Cheong et al. 2011), thus causing decreased supragranular synaptic activity that precedes granular spiking. However, close inspection of the data reveals that there are repetition-induced reductions in both granular currents as well as supragranular spiking preceding the significant reduction in supragranular currents that are trending toward significance. It thus seems most parsimonious to assume that the initial thalamocortical volley of activation is reduced when stimuli repeat, and intracortical adaptation effectively results in an amplification of these subtle sensory changes.

Suppression without increased inhibition. Another important conclusion derived from our study is that repetition suppression in V1 does not seem to be solely caused by active inhibition via increased feedback from higher level areas. Cortico-cortical long-range projections are mostly excitatory. The local effect of their activation thus should increase net depolarization. In other words, heightened feedback increases synaptic activation, resulting in a larger CSD response in the extragranular layers (see Cox et al. 2019; Spaak et al. 2012; van Kerkoerle et al. 2014, 2017). It is conceivable that the excitatory postsynaptic potentials evoked by excitatory cortical feedback and the inhibitory postsynaptic potentials evoked by subsequent interneuron activation cancel their respective electric fields in the extracellular medium. In this case, the result should cause little to no difference in evoked current sinks. Thus none of these processes sufficiently seems to explain the pronounced reduction in net depolarization in supragranular layers. The most parsimonious explanation for our finding therefore seems to be that there is reduced overall synaptic excitation in V1 when visual stimuli repeat. Having stated this, it should be noted that CSD alone cannot provide conclusive evidence regarding the precise synaptic mechanisms under-

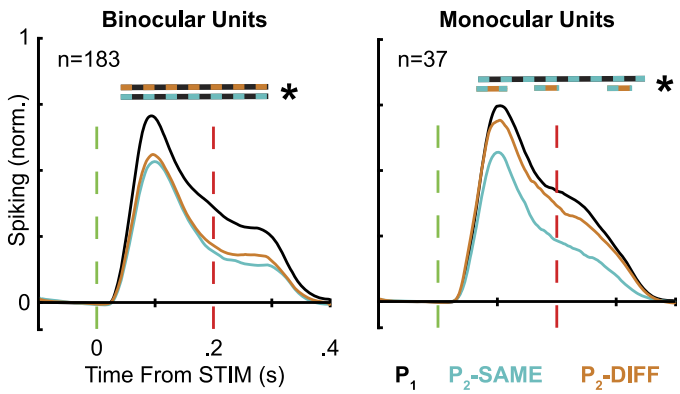

Fig. 11. V1 repetition suppression in response to stimulating opposite eyes for binocular and monocular V1 neurons. Data represent the smoothed, median normalized response of all units that fall in each respective category (n = no. of units). Black lines denote the response to initial presentation (P_1). In the case of monocular units, initial presentations were restricted to the dominant eye. Teal lines depict the response to the second presentation if the initial presentation was presented to the same eye (P_2-Same). Orange lines depict the response to the second presentation when the initial presentation was in the other eye (P2-Diff). *$P < 0.05$, time points (represented by striped horizontal bars) that were significant (paired-samples t-tests).

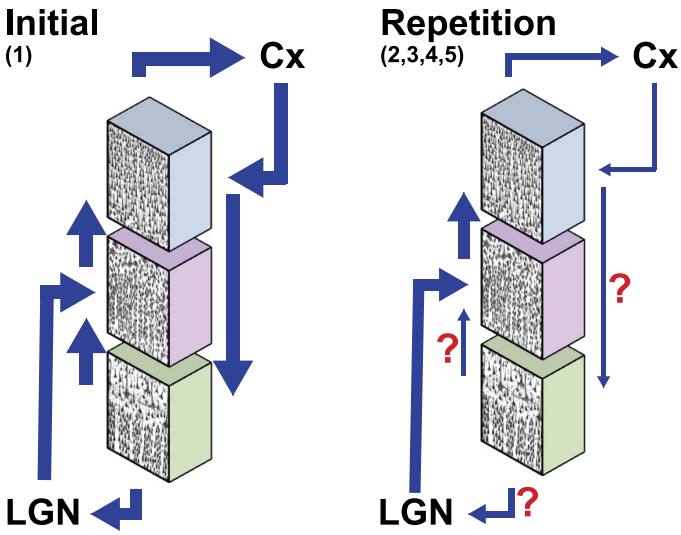

Fig. 12. Cartoon model of visual adaptation within V1's laminar microcircuit. *Left*: when a stimulus is first encountered (*1*), sensory activation initially mainly activates spiny stellate cells in the granular input layer 4C of V1 (pink). Layer 4C neurons predominantly project onto supragranular neurons (blue), whose activation spreads to other layers (green) and eventually to other visual areas downstream in the visual hierarchy. Intracortical spread of activation via horizontal connections as well as feedback from downstream areas to the extragranular layers of cortex can further enhance neuronal responses in these layers. *Right*: following stimulus repetition (*2*, *3*, *4*, *5*), intracortical activation is reduced, leading to reduced overall activity.

lying repetition suppression because it represents a spatially summed population signal.

Relationship to repetition suppression in extrastriate cortex. The phenomenon described in this article both resembles as well as differs from reports of repetition suppression in inferotemporal (IT) cortex, where the phenomenon was originally described (McMahon and Olson 2007; Miller et al. 1991, 1993; Miller and Desimone 1994). Both IT as well as V1 responses exhibit the greatest suppressive effect following the initial stimulus. However, IT neurons continue to adapt (i.e., further diminish their responses) with repeated presentations, whereas V1 neurons seem to maintain a more or less stable diminished response following the third stimulus repetition. Stimulus differences and other paradigmatic differences make it difficult to directly compare results obtained in these visual areas. Notably, we did not directly test adaptation relative to repeating identical stimuli as has been done in most examinations of IT cortex (but see Liu et al. 2009). However, the fact that a similar adaptive process is seen at both the initial cortical stage of visual processing as well as near the apex of the visual cortical hierarchy raises the question of how far areas that fall in between exhibit a similar profile of repetition suppression (see also Brunet et al. 2014; Patterson et al. 2014).

Potential role of expectation. Repetition suppression has been linked to predictive coding and expectation more generally (Auksztulewicz and Friston 2016; Summerfield et al. 2008). In this framework, reduced spiking responses to repeated stimuli are due to the reduction of a prediction error signal when probabilistic expectations about stimulus reoccurrence are met. We have not directly tested this hypothesis. One approach to test this hypothesis would be to alter the statistical distributions of stimulus occurrence. Single-neuron recordings in IT using such manipulations did not yield conclusive results (Bell et al. 2016; Kovács and Vogels 2014). We would expect our paradigm to evoke a certain prediction error given that at least one stimulus feature (orientation or ocularity) was randomly varied between presentation. This having been stated, it is noteworthy that our data seem compatible with a recently proposed model of predictive coding utilizing V1's columnar microcircuit (Bastos et al. 2012) in that we observed reduced synaptic activation in V1's feedback-recipient layers for repeated stimuli.

Note that we deliberately limited our study to the effects of stimulus repetition on sensory cortical activation. Previous studies have shown that spontaneous activity (i.e., ongoing spiking in between stimulus presentations) in sensory areas can be affected by stimulus history, as well (Bisley and Pasternak 2000; van Kerkoerle et al. 2017). Visual inspection of both the population spiking and LFP responses from our paradigm suggests that spontaneous activity during the ISIs was modulated by the task, as well. This finding may be related to neuronal entrainment (Lakatos et al. 2008; Morillon et al. 2016; Schroeder and Lakatos 2009) to rhythmic stimulation, which we intend to investigate in a separate study.

Possible role of attention. It is possible that the initial visual stimulation of each sequence draws stimulus-driven, exogenous attention toward the stimulus location, as reflected by increased neuronal firing. With subsequent stimuli, focused attention might fade or even be inhibited (i.e., by inhibition of return). As a result, neuronal responses would be expected to decline. We cannot entirely rule out this hypothesis because we did not control the animal's state of attention. However, behavioral performance generally increases with stimulus repetition, which goes counter to the assumption of a fading attentional focus (Tulving and Schacter 1990). It thus seems likely that attention does not play a significant role in repetition suppression and the associated effects we observed. This observation raises the interesting question whether and how visual selective attention and visual adaptation might interact on the laminar level in V1.

ACKNOWLEDGMENTS

We thank S. Amemori, Dr. T. Apple, M. Feurtado, K. George-Durrett, Dr. A. Graybiel, N. Halper, P. Henry, M. Johnson, Dr. C. Jones, M. Maddox, L. McIntosh, Dr. A. Newton, J. Parker, M. Schall, C. Thompson, K. Torab, M. Schall, E. A. Sigworth, C. Subraveti, B. Williams, R. Williams, and Dr. W. Zinke for technical advice and assistance. We thank Dr. J. D. Schall, B. M. Carlson, N. Valov, and K. A. Lowe for comments on an earlier version of the manuscript.

GRANTS

This work was supported by National Institutes of Health (NIH) Grants R01EY027402, T32EY007135 (to K. Dougherty and J. A. Westerberg), and P30EY008126. MRI scans were performed at the Vanderbilt University Institute of Imaging Science (VUIIS) Center for Human Imaging on a 3T scanner supported by NIH Grant S10OD021771. A. Maier is supported by a research grant from the Whitehall Foundation, a Career Starter grant from the Knights Templar Eye Foundation, and a fellowship from the Alfred P. Sloan Foundation.

DISCLOSURES

No conflicts of interest, financial or otherwise, are declared by the authors.

AUTHOR CONTRIBUTIONS

J.A.W. and A.M. conceived and designed research; J.A.W., M.A.C., and K.D. performed experiments; J.A.W., M.A.C., and K.D. analyzed data; J.A.W., M.A.C., K.D., and A.M. interpreted results of experiments; J.A.W. prepared figures; J.A.W. drafted manuscript; J.A.W., M.A.C., K.D., and A.M. edited and revised manuscript; J.A.W., M.A.C., K.D., and A.M. approved final version of manuscript.

REFERENCES

Albrecht DG, Farrar SB, Hamilton DB. Spatial contrast adaptation characteristics of neurones recorded in the cat's visual cortex. *J Physiol* 347: 713–739, 1984. doi:10.1113/jphysiol.1984.sp015092.

Anderson JC, Martin KA. The synaptic connections between cortical areas V1 and V2 in macaque monkey. *J Neurosci* 29: 11283–11293, 2009. doi:10.1523/JNEUROSCI.5757-08.2009.

Asaad WF, Eskandar EN. A flexible software tool for temporally-precise behavioral control in Matlab. *J Neurosci Methods* 174: 245–258, 2008. doi:10.1016/j.jneumeth.2008.07.014.

Auksztulewicz R, Friston K. Repetition suppression and its contextual determinants in predictive coding. *Cortex* 80: 125–140, 2016. doi:10.1016/j.cortex.2015.11.024.

Baccus SA, Meister M. Fast and slow contrast adaptation in retinal circuitry. *Neuron* 36: 909–919, 2002. doi:10.1016/S0896-6273(02)01050-4.

Barron HC, Garvert MM, Behrens TE. Repetition suppression: a means to index neural representations using BOLD? *Philos Trans R Soc Lond B Biol Sci* 371: 20150355, 2016. doi:10.1098/rstb.2015.0355.

Bastos AM, Loonis R, Kornblith S, Lundqvist M, Miller EK. Laminar recordings in frontal cortex suggest distinct layers for maintenance and control of working memory. *Proc Natl Acad Sci USA* 115: 1117–1122, 2018. doi:10.1073/pnas.1710323115.

Bastos AM, Usrey WM, Adams RA, Mangun GR, Fries P, Friston KJ. Canonical microcircuits for predictive coding. *Neuron* 76: 695–711, 2012. doi:10.1016/j.neuron.2012.10.038.

Baylis GC, Rolls ET. Responses of neurons in the inferior temporal cortex in short term and serial recognition memory tasks. *Exp Brain Res* 65: 614–622, 1987. doi:10.1007/BF00235984.

Bell AH, Summerfield C, Morin EL, Malecek NJ, Ungerleider LG. Encoding of stimulus probability in macaque inferior temporal cortex. *Curr Biol* 26: 2280–2290, 2016. doi:10.1016/j.cub.2016.07.007.

Benevento LA, Rezak M. The cortical projections of the inferior pulvinar and adjacent lateral pulvinar in the rhesus monkey (*Macaca mulatta*): an autoradiographic study. *Brain Res* 108: 1–24, 1976. doi:10.1016/0006-8993(76)90160-8.

Benjamini Y, Hochberg Y. Controlling the false discovery rate: a practical and powerful approach to multiple testing. *J R Stat Soc Series B Methodol* 57: 289–300, 1995.

Berry MJ 2nd, Brivanlou IH, Jordan TA, Meister M. Anticipation of moving stimuli by the retina. *Nature* 398: 334–338, 1999. doi:10.1038/18678.

Bisley JW, Pasternak T. The multiple roles of visual cortical areas MT/MST in remembering the direction of visual motion. *Cereb Cortex* 10: 1053–1065, 2000. doi:10.1093/cercor/10.11.1053.

Brunet NM, Bosman CA, Vinck M, Roberts M, Oostenveld R, Desimone R, De Weerd P, Fries P. Stimulus repetition modulates gamma-band synchronization in primate visual cortex. *Proc Natl Acad Sci USA* 111: 3626–3631, 2014. doi:10.1073/pnas.1309714111.

Casagrande VA. A third parallel visual pathway to primate area V1. *Trends Neurosci* 17: 305–310, 1994. doi:10.1016/0166-2236(94)90065-5.

Cheong SK, Tailby C, Martin PR, Levitt JB, Solomon SG. Slow intrinsic rhythm in the koniocellular visual pathway. *Proc Natl Acad Sci USA* 108: 14659–14663, 2011. doi:10.1073/pnas.1108004108.

Cox MA, Dougherty K, Adams GK, Reavis EA, Westerberg JA, Moore BS, Leopold DA, Maier A. Spiking suppression precedes cued attentional enhancement of neural responses in primary visual cortex. *Cereb Cortex* 29: 77–90, 2019. doi:10.1093/cercor/bhx305.

Cox MA, Dougherty K, Westerberg JA, Schall M, Maier A. Temporal dynamics of binocular integration in primary visual cortex. *J Vis*. In press.

Cox MA, Schmid MC, Peters AJ, Saunders RC, Leopold DA, Maier A. Receptive field focus of visual area V4 neurons determines responses to illusory surfaces. *Proc Natl Acad Sci USA* 110: 17095–17100, 2013. doi:10.1073/pnas.1310806110.

Dougherty K, Cox MA, Ninomiya T, Leopold DA, Maier A. Ongoing alpha activity in V1 regulates visually driven spiking responses. *Cereb Cortex* 27: 1113–1124, 2017. doi:10.1093/cercor/bhv304.

Dougherty K, Cox MA, Westerberg JA, Maier A. Binocular modulation of monocular V1 neurons. *Curr Biol* 29: 381–391.e4, 2019. doi:10.1016/j.cub.2018.12.004.

Douglas RJ, Martin KA. A functional microcircuit for cat visual cortex. *J Physiol* 440: 735–769, 1991. doi:10.1113/jphysiol.1991.sp018733.

Douglas RJ, Martin KA, Whitteridge D. Selective responses of visual cortical cells do not depend on shunting inhibition. *Nature* 332: 642–644, 1988. doi:10.1038/332642a0.

Felleman DJ, Van Essen DC. Distributed hierarchical processing in the primate cerebral cortex. *Cereb Cortex* 1: 1–47, 1991. doi:10.1093/cercor/1.1.1.

Garey LJ, Powell TP. An experimental study of the termination of the lateral geniculo-cortical pathway in the cat and monkey. *Proc R Soc Lond B Biol Sci* 179: 41–63, 1971. doi:10.1098/rspb.1971.0080.

Glickstein M, King RA, Miller J, Berkley M. Cortical projections from the dorsal lateral geniculate nucleus of cats. *J Comp Neurol* 130: 55–75, 1967. doi:10.1002/cne.901300104.

Godlove DC, Maier A, Woodman GF, Schall JD. Microcircuitry of agranular frontal cortex: testing the generality of the canonical cortical microcircuit. *J Neurosci* 34: 5355–5369, 2014. doi:10.1523/JNEUROSCI.5127-13.2014.

Gratiy SL, Halnes G, Denman D, Hawrylycz MJ, Koch C, Einevoll GT, Anastassiou CA. From Maxwell's equations to the theory of current-source density analysis. *Eur J Neurosci* 45: 1013–1023, 2017. doi:10.1111/ejn.13534.

Green DM, Swets JA. *Signal Detection Theory and Psychophysics*. New York: Wiley, 1966.

Halnes G, Mäki-Marttunen T, Pettersen KH, Andreassen OA, Einevoll GT. Ion diffusion may introduce spurious current sources in current-source density (CSD) analysis. *J Neurophysiol* 118: 114–120, 2017. doi:10.1152/jn.00976.2016.

Hansen BJ, Dragoi V. Adaptation-induced synchronization in laminar cortical circuits. *Proc Natl Acad Sci USA* 108: 10720–10725, 2011. doi:10.1073/pnas.1102017108.

Helmholtz H. *Handbuch der physiologischen Optik*. Leipzig, Germany: Leopold Voss, 1867.

Kaas JH, Lyon DC. Pulvinar contributions to the dorsal and ventral streams of visual processing in primates. *Brain Res Brain Res Rev* 55: 285–296, 2007. doi:10.1016/j.brainresrev.2007.02.008.

Kaliukhovich DA, Vogels R. Neurons in macaque inferior temporal cortex show no surprise response to deviants in visual oddball sequences. *J Neurosci* 34: 12801–12815, 2014. doi:10.1523/JNEUROSCI.2154-14.2014.

Kar K, Krekelberg B. Testing the assumptions underlying fMRI adaptation using intracortical recordings in area MT. *Cortex* 80: 21–34, 2016. doi:10.1016/j.cortex.2015.12.011.

Kim HG, Connors BW. Apical dendrites of the neocortex: correlation between sodium- and calcium-dependent spiking and pyramidal cell morphology. *J Neurosci* 13: 5301–5311, 1993. doi:10.1523/JNEUROSCI.13-12-05301.1993.

King JL, Lowe MP, Stover KR, Wong AA, Crowder NA. Adaptive processes in thalamus and cortex revealed by silencing of primary visual cortex during contrast adaptation. *Curr Biol* 26: 1295–1300, 2016. doi:10.1016/j.cub.2016.03.018.

Kobatake E, Tanaka K. Neuronal selectivities to complex object features in the ventral visual pathway of the macaque cerebral cortex. *J Neurophysiol* 71: 856–867, 1994. doi:10.1152/jn.1994.71.3.856.

Kohn A. Visual adaptation: physiology, mechanisms, and functional benefits. *J Neurophysiol* 97: 3155–3164, 2007. doi:10.1152/jn.00086.2007.

Kovács G, Vogels R. When does repetition suppression depend on repetition probability? *Front Hum Neurosci* 8: 685, 2014. doi:10.3389/fnhum.2014.00685.

Lakatos P, Karmos G, Mehta AD, Ulbert I, Schroeder CE. Entrainment of neuronal oscillations as a mechanism of attentional selection. *Science* 320: 110–113, 2008. doi:10.1126/science.1154735.

Li L, Miller EK, Desimone R. The representation of stimulus familiarity in anterior inferior temporal cortex. *J Neurophysiol* 69: 1918–1929, 1993. doi:10.1152/jn.1993.69.6.1918.

Liu Y, Murray SO, Jagadeesh B. Time course and stimulus dependence of repetition-induced response suppression in inferotemporal cortex. *J Neurophysiol* 101: 418–436, 2009. doi:10.1152/jn.90960.2008.

Logothetis NK, Kayser C, Oeltermann A. In vivo measurement of cortical impedance spectrum in monkeys: implications for signal propagation. *Neuron* 55: 809–823, 2007. doi:10.1016/j.neuron.2007.07.027.

Maier A. Neuroscience: the cortical layering of visual processing. *Curr Biol* 23: R959–R961, 2013. doi:10.1016/j.cub.2013.09.010.

Maier A, Adams GK, Aura CJ, Leopold DA. Distinct superficial and deep laminar domains of activity in the visual cortex during rest and stimulation. *Front Syst Neurosci* 4: 31, 2010. doi:10.3389/fnsys.2010.00031.

Markov NT, Vezoli J, Chameau P, Falchier A, Quilodran R, Huissoud C, Lamy C, Misery P, Giroud P, Ullman S, Barone P, Dehay C, Knoblauch K, Kennedy H. Anatomy of hierarchy: feedforward and feedback pathways in macaque visual cortex. *J Comp Neurol* 522: 225–259, 2014. doi:10.1002/cne.23458.

Mason A, Nicoll A, Stratford K. Synaptic transmission between individual pyramidal neurons of the rat visual cortex in vitro. *J Neurosci* 11: 72–84, 1991. doi:10.1523/JNEUROSCI.11-01-00072.1991.

McMahon DB, Olson CR. Repetition suppression in monkey inferotemporal cortex: relation to behavioral priming. *J Neurophysiol* 97: 3532–3543, 2007. doi:10.1152/jn.01042.2006.

Michelson AA. *Studies in Optics*. Chicago, IL: The University of Chicago Press, 1927.

Mignard M, Malpeli JG. Paths of information flow through visual cortex. *Science* 251: 1249–1251, 1991. doi:10.1126/science.1848727.

Miller EK, Desimone R. Parallel neuronal mechanisms for short-term memory. *Science* 263: 520–522, 1994. doi:10.1126/science.8290960.

Miller EK, Li L, Desimone R. A neural mechanism for working and recognition memory in inferior temporal cortex. *Science* 254: 1377–1379, 1991. doi:10.1126/science.1962197.

Miller EK, Li L, Desimone R. Activity of neurons in anterior inferior temporal cortex during a short-term memory task. *J Neurosci* 13: 1460–1478, 1993. doi:10.1523/JNEUROSCI.13-04-01460.1993.

Mitzdorf U. Current source-density method and application in cat cerebral cortex: investigation of evoked potentials and EEG phenomena. *Physiol Rev* 65: 37–100, 1985. doi:10.1152/physrev.1985.65.1.37.

Mitzdorf U. Properties of the evoked potential generators: current source-density analysis of visually evoked potentials in the cat cortex. *Int J Neurosci* 33: 33–59, 1987. doi:10.3109/00207458708985928.

Mitzdorf U, Singer W. Excitatory synaptic ensemble properties in the visual cortex of the macaque monkey: a current source density analysis of electrically evoked potentials. *J Comp Neurol* 187: 71–83, 1979. doi:10.1002/cne.901870105.

Morillon B, Schroeder CE, Wyart V, Arnal LH. Temporal prediction in lieu of periodic stimulation. *J Neurosci* 36: 2342–2347, 2016. doi:10.1523/JNEUROSCI.0836-15.2016.

Movshon JA, Lennie P. Pattern-selective adaptation in visual cortical neurones. *Nature* 278: 850–852, 1979. doi:10.1038/278850a0.

Nicholson C, Freeman JA. Theory of current source-density analysis and determination of conductivity tensor for anuran cerebellum. *J Neurophysiol* 38: 356–368, 1975. doi:10.1152/jn.1975.38.2.356.

Ninomiya T, Dougherty K, Godlove DC, Schall JD, Maier A. Microcircuitry of agranular frontal cortex: contrasting laminar connectivity between occipital and frontal areas. *J Neurophysiol* 113: 3242–3255, 2015. doi:10.1152/jn.00624.2014.

Ogren MP, Hendrickson AE. The distribution of pulvinar terminals in visual areas 17 and 18 of the monkey. *Brain Res* 137: 343–350, 1977. doi:10.1016/0006-8993(77)90344-4.

Ortiz G, Odom JV, Passaglia CL, Tzekov RT. Efferent influences on the bioelectrical activity of the retina in primates. *Doc Ophthalmol* 134: 57–73, 2017. doi:10.1007/s10633-016-9567-5.

Pachitariu M, Steinmetz NA, Kadir SN, Carandini M, Harris KD. Fast and accurate spike sorting of high-channel count probes with KiloSort. In: *Advances in Neural Information Processing Systems 29*, edited by Lee DD, Sugiyama M, Luxburg UV, Guyon I, Garnett R. Barcelona: Neural Information Processing Systems, 2016, p. 4448–4456.

Patterson CA, Duijnhouwer J, Wissig SC, Krekelberg B, Kohn A. Similar adaptation effects in primary visual cortex and area MT of the macaque monkey under matched stimulus conditions. *J Neurophysiol* 111: 1203–1213, 2014. doi:10.1152/jn.00030.2013.

Pettersen KH, Devor A, Ulbert I, Dale AM, Einevoll GT. Current-source density estimation based on inversion of electrostatic forward solution: effects of finite extent of neuronal activity and conductivity discontinuities. *J Neurosci Methods* 154: 116–133, 2006. doi:10.1016/j.jneumeth.2005.12.005.

Quiroga MDM, Morris AP, Krekelberg B. Adaptation without plasticity. *Cell Reports* 17: 58–68, 2016. doi:10.1016/j.celrep.2016.08.089.

Rezak M, Benevento LA. A comparison of the projections of the dorsal lateral geniculate nucleus, the inferior pulvinar and adjacent lateral pulvinar to striate cortex (area 17) in the macaque monkey. *Brain Res* 167: 19–41, 1979. doi:10.1016/0006-8993(79)90260-9.

Riches IP, Wilson FA, Brown MW. The effects of visual stimulation and memory on neurons of the hippocampal formation and the neighboring parahippocampal gyrus and inferior temporal cortex of the primate. *J Neurosci* 11: 1763–1779, 1991. doi:10.1523/JNEUROSCI.11-06-01763.1991.

Rockland KS, Pandya DN. Laminar origins and terminations of cortical connections of the occipital lobe in the rhesus monkey. *Brain Res* 179: 3–20, 1979. doi:10.1016/0006-8993(79)90485-2.

Rockland KS, Virga A. Terminal arbors of individual "feedback" axons projecting from area V2 to V1 in the macaque monkey: a study using immunohistochemistry of anterogradely transported *Phaseolus vulgaris*-leucoagglutinin. *J Comp Neurol* 285: 54–72, 1989. doi:10.1002/cne.902850106.

Romero MC, Castro AF, Bermudez MA, Perez R, Gonzalez F. Eye dominance and response latency in area V1 of the monkey. *Vis Neurosci* 24: 757–761, 2007. doi:10.1017/S0952523807070642.

Rosner B. Percentage points for a generalized ESD many-outlier procedure. *Technometrics* 25: 165–172, 1983. doi:10.1080/00401706.1983.10487848.

Sawamura H, Orban GA, Vogels R. Selectivity of neuronal adaptation does not match response selectivity: a single-cell study of the FMRI adaptation paradigm. *Neuron* 49: 307–318, 2006. doi:10.1016/j.neuron.2005.11.028.

Sayer RJ, Friedlander MJ, Redman SJ. The time course and amplitude of EPSPs evoked at synapses between pairs of CA3/CA1 neurons in the hippocampal slice. *J Neurosci* 10: 826–836, 1990. doi:10.1523/JNEUROSCI.10-03-00826.1990.

Schroeder CE, Lakatos P. Low-frequency neuronal oscillations as instruments of sensory selection. *Trends Neurosci* 32: 9–18, 2009. doi:10.1016/j.tins.2008.09.012.

Schroeder CE, Mehta AD, Givre SJ. A spatiotemporal profile of visual system activation revealed by current source density analysis in the awake macaque. *Cereb Cortex* 8: 575–592, 1998. doi:10.1093/cercor/8.7.575.

Self MW, van Kerkoerle T, Supèr H, Roelfsema PR. Distinct roles of the cortical layers of area V1 in figure-ground segregation. *Curr Biol* 23: 2121–2129, 2013. doi:10.1016/j.cub.2013.09.013.

Sobotka S, Ringo JL. Stimulus specific adaptation in excited but not in inhibited cells in inferotemporal cortex of macaque. *Brain Res* 646: 95–99, 1994. doi:10.1016/0006-8993(94)90061-2.

Sobotka S, Ringo JL. Mnemonic responses of single units recorded from monkey inferotemporal cortex, accessed via transcommissural versus direct pathways: a dissociation between unit activity and behavior. *J Neurosci* 16: 4222–4230, 1996. doi:10.1523/JNEUROSCI.16-13-04222.1996.

Sotero RC, Bortel A, Naaman S, Mocanu VM, Kropf P, Villeneuve MY, Shmuel A. Laminar distribution of phase-amplitude coupling of spontaneous current sources and sinks. *Front Neurosci* 9: 454, 2015. doi:10.3389/fnins.2015.00454.

Spaak E, Bonnefond M, Maier A, Leopold DA, Jensen O. Layer-specific entrainment of γ-band neural activity by the α rhythm in monkey visual cortex. *Curr Biol* 22: 2313–2318, 2012. doi:10.1016/j.cub.2012.10.020.

Summerfield C, Trittschuh EH, Monti JM, Mesulam MM, Egner T. Neural repetition suppression reflects fulfilled perceptual expectations. *Nat Neurosci* 11: 1004–1006, 2008. doi:10.1038/nn.2163.

Thompson KG, Hanes DP, Bichot NP, Schall JD. Perceptual and motor processing stages identified in the activity of macaque frontal eye field neurons during visual search. *J Neurophysiol* 76: 4040–4055, 1996. doi:10.1152/jn.1996.76.6.4040.

Thomson AM, Deuchars J, West DC. Large, deep layer pyramid-pyramid single axon EPSPs in slices of rat motor cortex display paired pulse and frequency-dependent depression, mediated presynaptically and self-facilitation, mediated postsynaptically. *J Neurophysiol* 70: 2354–2369, 1993a. doi:10.1152/jn.1993.70.6.2354.

Thomson AM, Deuchars J, West DC. Single axon excitatory postsynaptic potentials in neocortical interneurons exhibit pronounced paired pulse facilitation. *Neuroscience* 54: 347–360, 1993b. doi:10.1016/0306-4522(93)90257-G.

Tulving E, Schacter DL. Priming and human memory systems. *Science* 247: 301–306, 1990. doi:10.1126/science.2296719.

van Kerkoerle T, Self MW, Dagnino B, Gariel-Mathis MA, Poort J, van der Togt C, Roelfsema PR. Alpha and gamma oscillations characterize

feedback and feedforward processing in monkey visual cortex. *Proc Natl Acad Sci USA* 111: 14332–14341, 2014. doi:10.1073/pnas.1402773111.

van Kerkoerle T, Self MW, Roelfsema PR. Layer-specificity in the effects of attention and working memory on activity in primary visual cortex. *Nat Commun* 8: 13804, 2017. doi:10.1038/ncomms13804.

Victor JD. The dynamics of the cat retinal X cell centre. *J Physiol* 386: 219–246, 1987. doi:10.1113/jphysiol.1987.sp016531.

Zeater N, Cheong SK, Solomon SG, Dreher B, Martin PR. Binocular visual responses in the primate lateral geniculate nucleus. *Curr Biol* 25: 3190–3195, 2015. doi:10.1016/j.cub.2015.10.033.

Zhang B, Bi H, Sakai E, Maruko I, Zheng J, Smith EL 3rd, Chino YM. Rapid plasticity of binocular connections in developing monkey visual cortex (V1). *Proc Natl Acad Sci USA* 102: 9026–9031, 2005. doi:10.1073/pnas.0500280102.